Intersubband, interband transitions, and optical properties of two vertically coupled hemispherical quantum dots with wetting layers

Masoomeh Dezhkam[1,*], Abdolnasser Zakery[2], and Alireza Keshavarz[3]

[1]*Department of Physics, Marvdasht Branch, Islamic Azad University, Marvdasht, Iran*
[2]*Department of Physics, College of Sciences, Shiraz University, Shiraz 71946-84795, Iran*
[3]*Department of Physics, Shiraz University of Technology, Shiraz 71555-313, Iran*
**Corresponding author: dezh@miau.ac.ir*

Received August 16, 2016; accepted October 14, 2016; posted online November 16, 2016

The electron and heavy hole energy levels of two vertically coupled InAs hemispherical quantum dots/wetting layers embedded in a GaAs barrier are calculated numerically. As the radius increases, the electronic energies increase for the small base radii and decrease for the larger ones. The energies decrease as the dot height increases. The intersubband and interband transitions of the system are also studied. For both, a spectral peak position shift to lower energies is seen due to the vertical coupling of dots. The interband transition energy decreases as the dot size increases, decreases for the dot shapes with larger heights, and reaches a minimum for coupled semisphere dots.

OCIS codes: 190.4720, 160.4760.
doi: 10.3788/COL201614.121904.

Quantum dots (QDs) have been one of the important topics of research activities in recent years. These semiconductor nanostructures with discrete subbands have been used in applications such as quantum information processing[1] and infrared photodetectors[2]. Some of the recent works on the QDs are optical properties of a box-shaped QD[3], a spherical QD with a position-dependent effective mass[4], a multilayered spherical QD[5], exciton effects on the optical properties of a disk-like QD under electric[6] and magnetic[7] fields, optical properties of a hydrogenic impurity in an ellipsoidal QD with an electric field[8], electronic and optical properties of a conical QD[9], electronic and optical properties of a hemispherical QD (HQD)/wetting layer (WL) with and without hydrogenic impurities[10].

As presented in our previous work[10], the hemispherical shape has been observed for islands formed during the growth of InAs on a GaAs substrate by Leonard *et al.*[11]. Moreover, Solomon *et al.*[12] have reported vertically coupled InAs/GaAs QDs grown by molecular beam epitaxy in the Stranski–Krastanov growth mode. They have observed InAs QDs with a uniform size in the vertically coupled layers of QDs, contrary to QDs of a single-layer sample with different sizes. This size uniformity results in a spectral linewidth reduction. The other result of the vertically coupling of QDs is the spectral peak position shifts to lower energies. Vertically aligned arrays have also been used to enhance the performance of devices like QD light emitting diodes, lasers, or spectrometers, which suffer from a low gain or response in the presence of only one dot layer[13]. These results show the importance of the investigation of vertically coupled QDs, so we consider two vertically coupled HQDs (TVCHQDs) with WLs. The electronic structure of two vertically coupled pyramidal[13] and cylindrical[14] QDs have previously been investigated.

In this Letter, the electron and heavy hole energy levels of two vertically coupled InAs HQDs with WLs embedded in a GaAs barrier are obtained numerically using the finite element method. Our system is considered to interact with two electromagnetic fields: a weak probe and a strong control field. Then, the linear and third-order nonlinear susceptibilities of the probe field are calculated in the system influenced by the control field. The numerical results for the energy levels, transition energies, and optical properties of the system are presented. The intersubband and interband transition energies are calculated. The dot size and shape dependence of the electron energy levels and interband transition energies are studied. The optical properties of TVCHQDs/WLs are compared with a single HQD/WL.

We have considered two vertically coupled InAs HQDs on top of WLs embedded in a GaAs barrier. According to Ref. [12] vertically coupled InAs QDs in GaAs have been constructed experimentally by the molecular beam epitaxy growth-induced islanding process. Up to 10 vertically coupled island layers have been reported. They have deposited the epitaxial layers in a Varian Gen II molecular-beam epitaxy system using As_2 as the arsenic source and a V/III beam equivalent pressure ratio of 9. The InAs island region and all subsequent depositions have been conducted at 500°C. The InAs deposition rate and GaAs growth rate have been 0.19 μm/h. The energy levels of the system are calculated. The HQDs base radius and height are assumed to be 10 and 5 nm, respectively, corresponding to the experimental results[11], with a

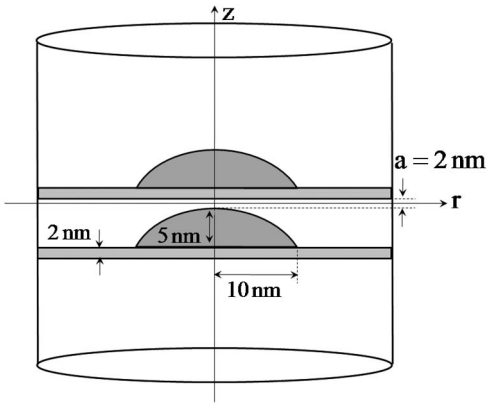

Fig. 1. Two vertically coupled InAs HQDs with WLs embedded in a GaAs barrier.

separation between QDs of $a = 2$ nm. This means that the GaAs spacer layer thickness, the thickness between two WLs, is 7 nm. Figure 1 shows the TVCHQDs/WLs system investigated in this Letter.

The strong confinement regime, in which the radius of the QD is much smaller than the exciton effective Bohr radius, is discussed. In this regime, the Coulomb term can be neglected. The Schrödinger equation in the effective mass approximation for a carrier (electron or heavy hole) confined to the TVCHQDs/WLs is given as

$$-\frac{\hbar^2}{2}\vec{\nabla}\cdot\left(\frac{1}{m^*(\mathbf{r})}\vec{\nabla}\psi(\mathbf{r})\right)+V(\mathbf{r})\psi(\mathbf{r})=E\psi(\mathbf{r}), \quad (1)$$

where $\hbar$ is the reduced Planck constant, $m^*(\mathbf{r})$ is the position-dependent carrier effective mass, and $V(\mathbf{r})$ is the confining potential. E and $\psi(\mathbf{r})$ are, respectively, the energy eigenvalue and wavefunction of the carrier which we have calculated by solving Eq. (1) numerically using the finite element method after the separation of $\psi(r,\phi,z)=Nu(r,z)e^{il\phi}$. N is the normalization constant and $|l|=0,1,2,\ldots$. The boundary conditions satisfied at the interface between the TVCHQDs/WLs and the barrier are[15]: $u|_{\mathrm{InAs}}=u|_{\mathrm{GaAs}}$ and $\mathbf{n}\cdot\vec{\nabla}(\frac{u}{m^*})|_{\mathrm{InAs}}=\mathbf{n}\cdot\vec{\nabla}(\frac{u}{m^*})|_{\mathrm{GaAs}}$.

$\mathbf{n}$ is the outer normal vector. The carrier effective masses and barrier potentials used in our calculations were: $m^*_{cl,\mathrm{InAs}}(r,z)=0.023m_0$, $m^*_{cl,\mathrm{GaAs}}(r,z)=0.067m_0$[16], $m^*_{hh,\mathrm{InAs}}(r,z)=0.41m_0$, and $m^*_{hh,\mathrm{GaAs}}(r,z)=0.5m_0$[17] ($m_0$ is the electron mass). $V_{\mathrm{InAs}}(r,z)=0$, $V_{el,\mathrm{GaAs}}(r,z)=0.697$ eV, and $V_{hh,\mathrm{GaAs}}(r,z)=0.288$ eV[18].

In this Letter, both the intersubband (intraband) and interband transitions are investigated. The intra(inter) band transition is between the electron ground and first excited states (heavy hole and electron ground states). The interband transition energy is the sum of the heavy hole, electron ground state energies (in the valence and conduction band, respectively), and the bandgap energy.

The optical properties of TVCHQDs/WLs induced by intersubband transitions in the conduction band are studied. The system is assumed to interact with two laser fields. Both fields are polarized along the x direction and propagate along the z direction. The matrix elements of the dipole moment $\mu_{ij}=|\langle u_i|e\hat{x}|u_j\rangle|$ ($\mu_{21}=0$, $\mu_{32}\neq 0$, and $\mu_{31}\neq 0$) have been numerically calculated using obtained eigenfunctions. e is the electronic charge, u_i is the wavefunction of the ith subband. The configuration of the three levels is a lambda type. The weak, pulsed probe (strong continuous-wave control) field is applied to transition $|1\rangle\leftrightarrow|3\rangle$ ($|2\rangle\leftrightarrow|3\rangle$) with the frequency of ω_p (ω_c).

Similar to our previous work[10], the first- and third-order susceptibilities of the probe pulse have been obtained. Since the absorption (dispersion) is proportional to the imaginary (real) part of the susceptibility[19], the first-order absorption and dispersion of the probe pulse are proportional to

$$\mathrm{Im}(\chi^{(1)}(\omega_p))=\frac{N'|\mu_{13}|^2}{2\varepsilon_0\hbar}\frac{\gamma_3(\Delta_p-\Delta_c)^2+\gamma_3\gamma_2^2+\gamma_2|\Omega_c|^2}{|B|^2}, \quad (2)$$

$$\mathrm{Re}(\chi^{(1)}(\omega_p))=\frac{N'|\mu_{13}|^2}{2\varepsilon_0\hbar}\times\frac{|\Omega_c|^2(\Delta_p-\Delta_c)-\Delta_p(\Delta_p-\Delta_c)^2-\Delta_p\gamma_2^2}{|B|^2}, \quad (3)$$

and the third-order absorption and dispersion are proportional to

$$\mathrm{Im}(\chi^{(3)}(\omega_p))=-\frac{N'|\mu_{13}|^4[|\Omega_c|^2+(\Delta_p-\Delta_c)^2+\gamma_2^2]}{24\varepsilon_0\hbar^3}\times\frac{[\gamma_3(\Delta_p-\Delta_c)^2+\gamma_3\gamma_2^2+\gamma_2|\Omega_c|^2]}{|B|^4}, \quad (4)$$

$$\mathrm{Re}(\chi^{(3)}(\omega_p))=-\frac{N'|\mu_{13}|^4[|\Omega_c|^2+(\Delta_p-\Delta_c)^2+\gamma_2^2]}{24\varepsilon_0\hbar^3}\times\frac{[(\Delta_p-\Delta_c)|\Omega_c|^2-\Delta_p(\Delta_p-\Delta_c)^2-\Delta_p\gamma_2^2]}{|B|^4}, \quad (5)$$

where $B=|\Omega_c|^2-(i\gamma_2+\Delta_p-\Delta_c)(i\gamma_3+\Delta_p)$. ε_0, N', and γ_i are, respectively, the permittivity of free space, the electron density, and the decay rate of subband $|i\rangle$. $\Delta_p=\omega_p-\omega_{31}$ and $\Delta_c=\omega_c-\omega_{32}$ are detunings of the probe and control fields (ω_{31} and ω_{32} are the transition frequencies of transitions $|3\rangle\leftrightarrow|1\rangle$ and $|3\rangle\leftrightarrow|2\rangle$). $2\Omega_p=\frac{\mu_{31}E_p}{\hbar}$ and $2\Omega_c=\frac{\mu_{32}E_c}{\hbar}$ are the Rabi frequencies associated with the coupling of the light fields to the transitions $|3\rangle\leftrightarrow|1\rangle$ and $|3\rangle\leftrightarrow|2\rangle$[20–22] ($\mu_{31}$ and μ_{32} are the matrix elements of the dipole moment for the corresponding transitions, $E_{p,c}$ is the slowly varying envelope of the fields).

The three lowest electron energy levels of the TVCHQDs/WLs system have been obtained by solving Eq. (1) numerically. The ground, first, and second excited state energies are 193.1, 206.8, and 305.7 meV, respectively. The electron is present in both of the two QDs because the two QDs are coupled together.

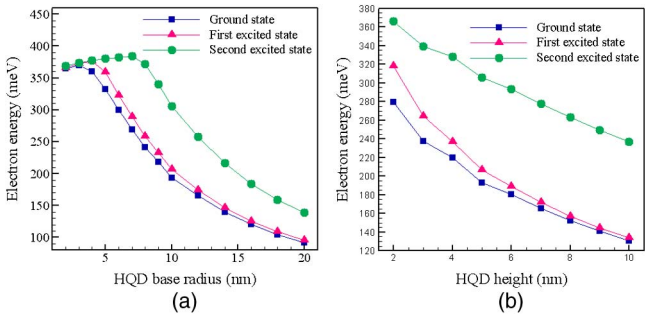

Fig. 2. Electron ground, first, and second excited state energy eigenvalues versus HQD (a) base radius and (b) height for TVCHQDs/WLs.

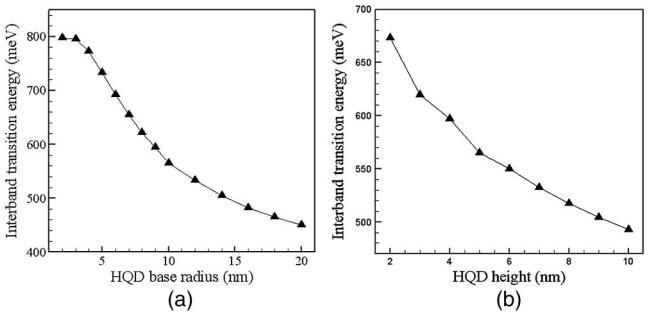

Fig. 3. Interband transition energy versus HQD (a) base radius and (b) height for TVCHQDs/WLs.

Under the condition that transition between the electron ground and first exited states is allowed, the intersubband transition energy is 13.7 meV. The corresponding value for the single HQD (base radius 10 nm, height 5 nm) in our previous work[10] was 110 meV. This shows a redshift due to the vertical coupling of HQDs.

As we know, the electronic structure of QD systems depends on the size of the dots, so HQDs with different base radii have been considered. For all HQDs, the base radius to height ratio is 2. The three lowest electron energy levels for TVCHQDs/WLs have been calculated. The ground, first, and second excited state energies as a function of the base radius are shown in Fig. 2(a). As the radius increases, the energies increase for the small base radii and decrease for the larger base radii. The reason can be explained according to the calculated electron wave functions. For small base radii, the electron wave function expands in both HQDs and WLs; however, for the larger radii, it localizes only in the HQDs. It is clear that, for the latter case, the energies should decrease as the dot size increases.

To investigate the dot shape dependence of the electronic structure of our system, we have considered HQDs with a base radius of 10 and $a = 2$ nm. We have changed the HQD height from 2 nm (oblate HQD) to 10 nm (semisphere QD) and calculated the electronic structure. The three lowest energy levels of the TVCHQDs/WLs as a function of height are shown in Fig. 2(b). It is clear that the energies decrease as the HQD height increases.

To investigate the interband transitions, the heavy hole energy levels in the valence band have been calculated by solving Eq. (1). For the TVCHQDs/WLs system shown in Fig. 1, an interband transition energy of 565.1 meV has been obtained. For comparison, the interband transition energy for a single HQD/WL with a base radius of 10 nm and a height of 5 nm has been calculated. The corresponding value is 571.9 meV. This shows a spectral peak position shift to lower energies due to the vertical coupling of HQDs. This transition energy reduction is in agreement with the experimental result obtained by Solomon *et al.*[12].

Figure 3(a) shows the interband transition energy of the TVCHQDs/WLs as a function of the HQD base radius. The interband transition energy decreases as the HQDs size increases.

Figure 3(b) shows the interband transition energy of the TVCHQDs/WLs as a function of the HQD height. As we can see, the interband transition energy varies for different shapes of dots. Oblate coupled QDs systems have the maximum interband transition energy. The interband transition energy decreases as the height increases and reaches a minimum value for coupled semisphere QDs.

Finally, we want to study the optical properties of the TVCHQDs/WLs shown in Fig. 1 and compare them to the single HQD/WL investigated in our previous work with the same size[10]. The linear and nonlinear absorptions and dispersions of the probe pulse as a function of the probe frequency ω_p for these two systems are shown in Fig. 4. The parameters used in the calculations are: $N'=3\times10^{22}\,\mathrm{m}^{-3}$[3], $\Omega_c = 9\times10^{12}\ \mathrm{s}^{-1}$, $\gamma_2 = \gamma_3 = 10^{12}\ \mathrm{s}^{-1}$, and $\Delta_c = 2\gamma_2$.

As Fig. 4 shows, the linear and nonlinear absorptions and dispersions of the TVCHQDs/WLs exhibit blueshifts with respect to a single HQD/WL. The reason is the configuration of the lambda type for TVCHQDs/WLs in contrast with the configuration of a cascade type for

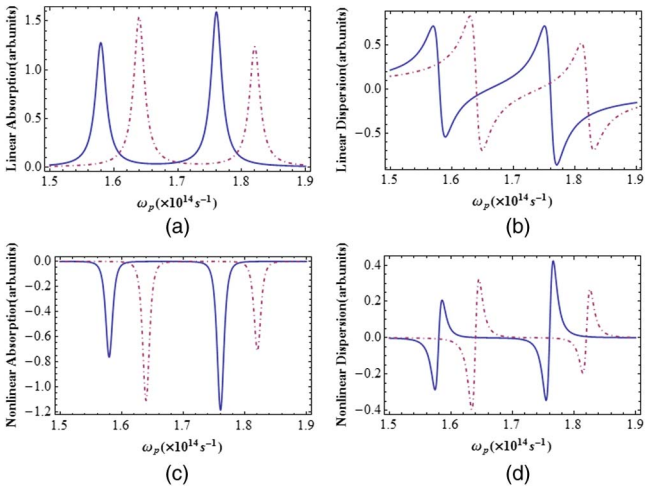

Fig. 4. Linear (a) absorption and (b) dispersion, and nonlinear (c) absorption and (d) dispersion of the probe pulse as a function of the probe frequency ω_p. The solid and dot-dashed lines correspond to single HQD/WL and TVCHQDs/WLs, respectively.

the single HQD/WL. For TVCHQDs/WLs, the $|1\rangle \leftrightarrow |3\rangle$ transition is induced by the probe field polarized along the x direction, whereas the $|1\rangle \leftrightarrow |2\rangle$ transition is induced in the case of a single HQD/WL. The larger transition frequency of TVCHQDs/WLs leads to the blue shift.

In conclusion, the electron and heavy hole energy levels of two vertically coupled InAs HQDs with WLs embedded in a GaAs barrier are calculated in the strong confinement regime. The energy levels are calculated by solving the Schrödinger equation numerically in the effective mass approximation using the finite element method. First, the electron energy levels in the conduction band were studied. Our calculations for different HQD sizes show that as the radius increases the electron ground, first, and second excited state energies increase for the small base radii and decrease for the larger base radii. For different QD shapes, the results show that the electron ground, first, and second excited state energies decrease as the HQD height increases. Then, both the intersubband and interband transition energies are obtained. Both of them show a spectral peak position shift to lower energies for the TVCHQDs/WLs with respect to a similar single HQD/WL. This is an important result of the vertical coupling of HQDs. The results show that the interband transition energy decreases as the HQD base radius and height are increase. Furthermore, the linear and third-order nonlinear absorptions and dispersions of the weak probe pulse propagating in the system influenced by a strong control field are obtained. A comparison of the optical properties of the TVCHQDs/WLs with that of a single HQD/WL shows that the linear and nonlinear absorptions and dispersions exhibit blueshifts.

References

1. E. Biolatti, I. D'Amico, P. Zanardi, and F. Rossi, Phys. Rev. B **65**, 075306 (2002).
2. H. C. Liu, Opto-Electron. Rev. **11**, 1 (2003).
3. S. Ünlü, İ. Karabulut, and H. Şafak, J. Phys. E **33**, 319 (2006).
4. A. Keshavarz and N. Zamani, Superlattices Microstruct. **58**, 191 (2013).
5. M. J. Karimi, G. Rezaei, and M. Nazari, J. Lumin. **145**, 55 (2014).
6. W. Xie, Opt. Commun. **283**, 1381 (2010).
7. L. Lu and W. Xie, Superlattices Microstruct. **50**, 40 (2011).
8. T. Chen, W. Xie, and Sh. Liang, J. Phys. E **44**, 786 (2012).
9. M. Dezhkam and A. Zakery, Chin. Opt. Lett. **10**, 121901 (2012).
10. M. Dezhkam and A. Zakery, J. Phys. B **443**, 70 (2014).
11. D. Leonard, K. Pond, and P. M. Petroff, Phys. Rev. B **50**, 11687 (1994).
12. G. S. Solomon, J. A. Trezza, A. F. Marshall, and J. S. Harris, Phys. Rev. Lett. **76**, 952 (1996).
13. G. Liang, S. Yong-chun, X. Jing-jun, and W. Zhan-guo, Superlattices Microstruct. **61**, 81 (2013).
14. B. Szafran, Acta Phys. Pol. A **114**, 1013 (2008).
15. F. Gelbard and K. J. Malloy, J. Comput. Phys. **172**, 19 (2001).
16. S. S. Li, J. B. Xia, Z. L. Yuan, and Z. Y. Xu, Phys. Rev. B **54**, 11575 (1996).
17. E. H. Li, J. Phys. E **5**, 215 (2005).
18. Y. T. B. Ali, G. Bastard, and R. Bennaceur, J. Phys. E **27**, 67 (2005).
19. K. J. Kuhn, G. U. Iyengar, and S. Yee, J. Appl. Phys. **70**, 5010 (1991).
20. Y. Wu and L. Deng, Opt. Lett. **29**, 2064 (2004).
21. Y. Wu and X. Yang, Phys. Rev. A **71**, 053806 (2005).
22. J. Li, R. Yu, J. Liu, P. Huang, and X. Yang, J. Phys. E **41**, 70 (2008).